THE JOURNAL OF PHYSICAL CHEMISTRY C

Article

pubs.acs.org/JPCC

Unifying Kinetic and Thermodynamic Analysis of 2 e⁻ and 4 e⁻ Reduction of Oxygen on Metal Surfaces

Heine A. Hansen,* Venkatasubramanian Viswanathan, and Jens K. Nørskov*

SUNCAT, SLAC National Accelerator Laboratory, Menlo Park, California 94025-7015, United States

Department of Chemical Engineering, Stanford University, Stanford, California, 94305-3030, United States

Supporting Information

ABSTRACT: Oxygen electrochemistry has played a key role in developing the foundational understanding of surface electrocatalysis. In this work, we develop a detailed microkinetic model for the oxygen reduction reaction based on density functional theory calculations and molucular dynamics simulations. The developed microkinetic model has a reaction order of 1 in O_2 and a 59 mV/dec Tafel slope in the potential range where the Pt(111) surface is dominated by OH adsorption. Using calculated scaling and Brønsted−Evans−Polanyi relations, we extend this analysis to calculate the activity on materials with a varying OH binding energy. We demonstrate the existence of a kinetic activity volcano which is in close agreement with the thermodynamic activity volcano derived earlier. Both of these analyses identify an activity optimum around 0.1 eV weaker binding of OH relative to Pt(111). The predictions of the kinetic activity volcano are in close agreement with several RDE experiments on metals and Pt alloys. On the basis of rate control analysis and Sabatier analysis, we demonstrate the close connection between the kinetic and thermodynamic formulations for oxygen reduction. We further examine trends in 2e⁻ reduction of O_2 to H_2O_2 and show a similar correspondence between the thermodynamic and kinetic activity volcano with the activity optimum around 0.3 eV weaker OH binding than Pt(111). On the basis of rate control analysis, we show that many elementary steps play a key role in determining the selectivity. This emphasizes the importance of detailed kinetic analysis for addressing trends in selectivity.

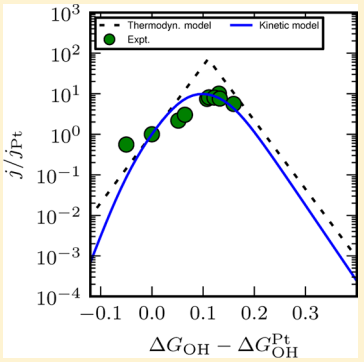

INTRODUCTION

The oxygen reduction reaction (ORR) has been a subject of major interest in electrochemistry owing to its technological and scientific importance.[1] Its technological importance stems from the fact that it constitutes the cathode reaction in a fuel cell and the sluggish kinetics associated with this reaction, even on the best precious-metal based catalysts, has limited a widespread adoption of PEM fuel cells. Scientifically, this reaction, along with the hydrogen electrochemistry, has served as the favorites in the development of an understanding of surface electrocatalysis.[2]

The fundamental understanding of the ORR has been largely based on the surface science approach to electrocatalysis.[2−14] The surface science approach relies on pure metal single crystals and well-characterized bulk alloys which are used as model systems for commercial electrocatalysts. These model systems can be characterized through various surface analytical tools and X-ray techniques, such as low energy electron diffraction (LEED), Auger electron spectroscopy (AES), X-ray photoelectron spectroscopy (XPS), low energy ion scattering (LEIS), X-ray absorption near-edge structure (XANES), extended X-ray absorption fine structure (EXAFS) and scanning tunneling microscopy (STM) in addition to traditional electrochemical and analytical tools, such as linear sweep voltammetry and *in situ* infrared spectroscopy.[2,11,14−21] The experimental techniques may be complemented by first principles calculations to explore the stability of adsorbate structures at the catalyst interface and examine reaction pathways.[22−31]

The most popular model system has been the Pt(111) surface, because terraces are believed to contain the active sites on Pt nanoparticles,[32−36] despite the fact stepped single crystals show higher activity than Pt(111) in $HClO_4$.[9] On the basis of the surface science approach, empirical and semiempirical kinetic models have been developed by Markovic and co-workers by fitting kinetic parameters to experimental data.[37,38] These models have emphasized the importance of site-blocking by the strongly adsorbing OH* adsorbate. In addition, it has been concluded that the first electron transfer step to O_2 is the rate-limiting step.[1,39]

The surface science approach has allowed the bridging of theory and experiment by enabling direct theoretical investigations of the reaction mechanism of oxygen reduction reaction on model systems.[2] Density functional theory calculations have been employed to calculate the adsorption energy of intermediates accounting for water stabilization, electric field effects, and entropic corrections.[40,41] These calculations can be used to construct free energy diagrams and a useful parameter, termed the thermodynamic limiting potential, can be extracted from these free energy diagrams.[40,42]

Received: October 9, 2013
Revised: March 5, 2014
Published: March 5, 2014

   dx.doi.org/10.1021/jp4100608 | J. Phys. Chem. C 2014, 118, 6706−6718

The thermodynamic limiting potential for a reduction reaction is defined as the highest potential where the entire reaction scheme is downhill in free energy. On the basis of this thermodynamic analysis, it has been demonstrated that the thermodynamic bottleneck for oxygen reduction reaction on Pt(111) is the reduction of OH* to water.[42] In this thermodynamic picture for oxygen reduction, the catalytic activity relative to Pt(111) can be enhanced by weakening the binding energy of O* or OH*.[14,40] However, beyond a certain weakening, due to correlated binding between OH* and OOH*,[43] it becomes thermodynamically uphill to activate O_2 as OOH* and this leads to a Sabatier volcano with the optimal catalyst striking a balance between these two reaction steps.[44] This thermodynamic picture has been successful in rationalizing trends in oxygen reduction[40,44] and recently in addressing trends in selectivity between the $2e^-$ vs $4e^-$ reduction of oxygen.[45] It has also been successful in explaining trends for hydrogen evolution,[46] oxygen evolution[47] and CO_2 reduction[48] and in select cases has been used to aid the identification of new active catalysts.[42,49]

While the kinetic picture of oxygen reduction on Pt(111) assigns the rate limiting step to the first electron transfer step, the thermodynamic picture assigns the thermodynamically limiting step to the reduction of OH* to water. An attempt to resolve this discrepancy was carried out by Rossmeisl et al.,[50] based on a phenomenological model. In the present work, we take this analysis a step further and develop a detailed kinetic model using free energy barriers based on density functional theory calculations and molecular dynamics simulations. We demonstrate that the developed model reproduces the experimental Tafel slope of 59 mV/dec and reaction order with respect to O_2 of 1. We use scaling relations, which relates the binding energies of intermediates with each other, and BEP relations, which relates activation energies to reaction energies, to extend our kinetic model to materials with varying OH (or O) binding energy. We demonstrate the existence of a kinetic activity volcano which is in close agreement with the thermodynamic activity volcano. Both of these analyses identify an optimum activity for 0.1 eV weaker OH binding than Pt(111) (or 0.2 eV weaker for O). We further carry out rate control analysis and demonstrate the close connection between the kinetic and thermodynamic formulations. Finally, we examine trends in $2e^-$ reduction of O_2 to H_2O_2 and show a similar correspondence between the thermodynamic and kinetic activity volcano. On the basis of rate control analysis, we show that several elementary steps play a key role in determining the selectivity. We suggest that such detailed kinetic analysis is necessary to address trends in selectivity, which are particular important for multielectron electrochemical reactions such as CO_2 reduction.

METHODS

In this section, we begin by describing our model for the active site and the general reaction mechanism for oxygen reduction considered in this study. Following this, we discuss briefly the methodology to calculate reaction free energies of electrochemical reactions.

Model of the Active Site. ORR intermediates such as OOH and OH are significantly stabilized by participating in a hydrogen bonded network on a catalyst surface. Therefore, these adsorbates prefer to bind on sites which are in registry with the lattice of extended hydrogen bonded networks.[51,52] However, when the O−O bond is broken in a chemical step, calculations have shown the dissociation products may move to interstitial sites which are out of registry with the hydrogen bonded network.[52] Figure 1 shows the example of OOH

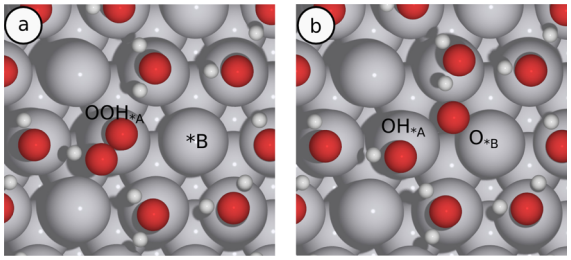

Figure 1. Surface model of the active sites on Pt(111): (a) $OOH*_A$ adsorbed in the mixed H_2O−OH layer with a vacant Pt $*_B$ site; (b) $OOH*_A$ dissociated to $OH*_A$ and $O*_B$.

dissociation to O and OH. Adsorbates formed on the interstitial sites, are less stable than intermediates within the hydrogen bonding network due to weaker hydrogen bonding and repulsion from adsorbates within the hydrogen bonding network. Motivated by these observations, we consider two different active surface sites in our model: lattice sites, $*_A$, which has optimum hydrogen bond stabilization, and interstitial sites, $*_B$, which has limited or no hydrogen bond stabilization. In order to optimize hydrogen bonding with solvating water molecules, adsorbates such as OOH_{*A} and OH_{*A} are well separated and interactions between adsorbates at the $*_A$ sites are expected to be small and we therefore treat the adsorbates as effectively noninteracting. However, the effect of solvation and hydrogen bonding is explicitly included in the calculated binding energies and activation energies. This approach is supported by the fact that the OH adsorption isotherm on Pt(111) in an effective noninteracting Langmuir model resembles the isotherm of a Monte Carlo based model including nearest neighbor adsorbate interactions.[24] The interstitial sites provide free sites required for the dissociation of the O−O bond, which in a kinetic model would otherwise be strongly suppressed on the surface blocked with OH. We take the $*_A$ sites to be saturated at $^1/_3$ ML coverage of OH, since this structure is found to be particularly stable.[52,53] Each $*_A$ site in this structure is associated with an interstitial $*_B$ site, and one Pt site blocked by a solvating water molecule. Adsorption of O_2 and formation of OOH on the interstitial sites in the hydrogen bonded network is thermodynamically difficult due to unfavorable adsorption geometry, repulsions from adsorbates on lattice sites, and poor hydrogen bonding. Therefore, we neglect the formation of these adsorbates on the interstitial sites.

Reaction Pathways. We employ a general kinetic model for the oxygen reduction reaction motivated by previous DFT calculations without *a priori* assumptions about rate-determining steps. In this model, O_2 molecules diffuse from the bulk electrolyte to the catalyst-electrolyte interface, given by,

$$O_2(aq) \underset{k_{-1}}{\overset{k_1}{\rightleftharpoons}} O_2(dl) \tag{1}$$

O_2 may then adsorb on free lattice sites and participate in the hydrogen bonded network and this is given by

$$O_2(dl) + *_A \underset{k_{-2}}{\overset{k_2}{\rightleftharpoons}} O_2*_A \tag{2}$$

dx.doi.org/10.1021/jp4100608 | J. Phys. Chem. C 2014, 118, 6706−6718

Once adsorbed on the surface, O_2 can be reduced to H_2O by a series of proton-coupled electron transfer steps in the associative pathway[40]

$$O_2{*_A} + H^+ + e^- \underset{k_{-3}}{\overset{k_3}{\rightleftharpoons}} OOH{*_A} \tag{3}$$

$$OOH{*_A} + H^+ + e^- \underset{k_{-4}}{\overset{k_4}{\rightleftharpoons}} O{*_A} + H_2O \tag{4}$$

$$O{*_A} + H^+ + e^- \underset{k_{-5}}{\overset{k_5}{\rightleftharpoons}} OH{*_A} \tag{5}$$

$$OH{*_A} + H^+ + e^- \underset{k_{-6}}{\overset{k_6}{\rightleftharpoons}} {*_A} + H_2O \tag{6}$$

We also include the dissociation of O_2 in a direct chemical step leading to two oxygen atoms adsorbed on a lattice and interstitial site, respectively.[30,40,54] This is given by

$$O_2{*_A} + {*_B} \underset{k_{-7}}{\overset{k_7}{\rightleftharpoons}} O{*_A} + O{*_B} \tag{7}$$

The oxygen adsorbed on the interstitial $*_B$ sites can be subsequently reduced to H_2O, given by

$$O{*_B} + H^+ + e^- \underset{k_{-8}}{\overset{k_8}{\rightleftharpoons}} OH{*_B} \tag{8}$$

$$OH{*_B} + H^+ + e^- \underset{k_{-9}}{\overset{k_9}{\rightleftharpoons}} {*_B} + H_2O \tag{9}$$

Rather than by the electrochemical reduction of OOH as in eq 4, OOH can also dissociate in a chemical step, given by

$$OOH{*_A} + {*_B} \underset{k_{-10}}{\overset{k_{10}}{\rightleftharpoons}} OH{*_A} + O{*_B} \tag{10}$$

Alternatively, OOH can be reduced to H_2O_2

$$OOH{*_A} + H^+ + e^- \underset{k_{-11}}{\overset{k_{11}}{\rightleftharpoons}} H_2O_2{*_A} \tag{11}$$

The H_2O_2 formed can dissociate or desorb from the catalyst surface and these steps are given below

$$H_2O_2{*_A} + {*_B} \underset{k_{-12}}{\overset{k_{12}}{\rightleftharpoons}} OH{*_A} + OH{*_B} \tag{12}$$

$$H_2O_2{*_A} \underset{k_{-13}}{\overset{k_{13}}{\rightleftharpoons}} {*_A} + H_2O_2 \tag{13}$$

The desorption of H_2O_2 leads to an overall $2e^-$ reduction of oxygen. We neglect diffusion of O and OH between $*_A$ and $*_B$ sites because $O*_B$ and $OH*_B$ are thermodynamically unstable and their reductive removal is already fast resulting in very low coverages of $O*_B$ and $OH*_B$. It has been verified that including diffusion of O and OH do not affect the calculated rates.

Reaction Free Energies. Reaction free energies of electrochemical reaction steps are calculated based on the computational standard hydrogen electrode formulation.[40] This formulation invokes the condition that at 0 V versus RHE, protons and electrons are in equilibrium with H_2 at standard pressure. This condition allows the free energy of an electrochemical step, ΔG_i, to be written as

$$\Delta G_i = \Delta G_i^0 + eU \tag{14}$$

where ΔG_i^0 is the reaction free energy at 0 V versus the reversible hydrogen electrode (RHE) and U is the potential measured against the reversible hydrogen electrode.

Scaling Relations. The binding energy of the reaction intermediates of oxygen reduction, O_2, OOH, O, OH and H_2O_2 are correlated and these binding energies are known to scale linearly with each other.[40,43,44,55−58] Following previous trend studies, we assume variations in free energy contributions are dominated by variations in the binding energy.[40,44] The variation in the free energy of intermediates can then be calculated from the difference in free energy of OH relative to Pt(111)[56]

$$G_{X*} = G_{X*}^{Pt} + \xi_X(G_{OH*} - G_{OH*}^{Pt}) \tag{15}$$

Scaling coefficients, ξ_X, are evaluated from previous DFT calculations and summarized in Table 1 together with reaction free energies calculated on Pt(111).

Table 1. Free Energy of Reaction Intermediates on Pt(111) at 0.9 V vs RHE, G^{Pt}, and the Scaling Coefficient, ξ

X	G_X^{Pt}/eV	ξ_X
O_2(aq), O_2(dl)	1.59	–
O_2*_A	1.39	1.2[56,57]
$OOH*_A$	1.21	1[44,59]
$O*_A$	−0.10	2[43,59]
$OH*_A$	−0.15	1
$H_2O_2*_A$	1.53	0.04[56,57]
$O*_B$	0.53	2[43,59]
$OH*_B$	0.20	1
H_2O_2(aq)	1.86	–
$*_A$, $*_B$	0.00	–

Rate Constants. According to transition state theory, the rate constant is given by

$$k_i = \frac{k_B T}{h} \exp\left(-\frac{G_{a,i}}{k_B T}\right) \tag{16}$$

where $G_{a,i}$ is the activation free energy. For chemical dissociation steps, we neglect the activation entropy and use activation energies calculated by Tripkovic et al. for the solvated Pt(111) surface.[52] We use Brønsted−Evans−Polanyi (BEP) relations derived from previously published DFT calculations to describe variations in the activation free energy with variations in the dissociation free energy relative to platinum.[56,57] With these approximations, the activation free energy is given by

$$G_{a,i} \approx E_{a,i}^{Pt} + \gamma_i(\Delta G_i - \Delta G_i^{Pt}) \tag{17}$$

where $E_{a,i}^{Pt}$ is the activation energy on Pt(111), $\Delta G_i - \Delta G_i^{Pt}$ is the reaction free energy of the step relative to Pt(111), and γ_i is the BEP slope. $E_{a,i}^{Pt}$, ΔG_i^{Pt} and γ_i are shown in Table 2.

The rate constants of an electrochemical reduction step, i, is assumed to take the functional form

$$k_i = \frac{k_B T}{h} \exp\left(-\frac{G_{a,i}^0}{k_B T}\right) \exp\left(-\frac{e\beta_i(U - U_i^0)}{k_B T}\right) \tag{18}$$

where $G_{a,i}^0$ is the activation free energy at the reversible potential of the step, U_i^0. The reversible potential of step i

$$U_i^0 = -\frac{\Delta G_i^0}{e} \tag{19}$$

dx.doi.org/10.1021/jp4100608 | J. Phys. Chem. C 2014, 118, 6706−6718

Table 2. Kinetic and Thermodynamic Parameters for Chemical Steps[a]

step	ν_i/s^{-1}	$E_{a,i}^{Pt}/eV$	$\Delta G_i^{Pt}/eV$	γ_i
(1)	8×10^5	0.00	0.00	–
(2)	1.00×10^8	0.00	−0.20	–
(7)	6.21×10^{12}	0.48	−0.93	0.69[57]
(10)	6.21×10^{12}	0.37	−0.83	0.39[57]
(12)	6.21×10^{12}	0.46	−1.49	0.19[57]
(13)	1.00×10^8	0.00	0.32	–

[a]The rate constant in eq 16 may here be calculated from $k_i = \nu_i \exp(-(E_a)/(k_BT))$. The low prefactors for steps (2) and (13) are caused by solvent reorganisation for the adsorption-desorption steps of O_2 and H_2O_2.

may be calculated from reaction free energies on Pt(111) listed in Table 1 and employing the scaling relations in eq 15. The reversible potential of a step is also the potential where the step is thermoneutral in free energy and therefore corresponds to the limiting potential of the step. Following other theoretical trend studies we assume β_i and $G_{a,i}^0$ are independent of material such that all variations in rate constants between materials are described by their variations in the reversible potentials for the various reaction steps.[48,60] We further assume that the activation free energy at the reversible potential, $G_{a,i}^0$, is independent of the reaction, such that the most exergonic reactions tend to have the lowest activation free energies in our model. For the reduction of OH to H_2O, DFT studies by Tripkovic et al. have found $\beta_i = 0.5$ and activation energy $E_{a,i}^0 = 0.26$ eV.[52] However, due to the presence of the water solvent, there is an additional energetic contribution from the requirement for the reorganization of solvent molecules around the reaction center undergoing the proton-coupled electron transfer. Recently, using molecular dynamics simulations, Limmer et al. studied the solvent reorganization at the Pt(111)−H_2O interface. They showed that solvent reorganization at the interface is significantly slower than in the bulk liquid. This is due to the binding of water to the Pt surface and commensurability of the preferred hydrogen bonding pattern and the Pt surface.[61] They estimated the time scale of surface reorganization, as calculated from the decorrelation time, to be around 1−10 ns. These interfacial relaxations are not included in DFT simulations, and consequently we write eq 18 in the form

$$k_i = A_i \exp\left(-\frac{E_{a,i}^0}{k_BT}\right)\exp\left(-\frac{e\beta_i(U - U_i^0)}{k_BT}\right) \tag{20}$$

where $E_{a,i}^0$ is the activation energy at the reversible potential calculated from DFT by Tripkovic et al., and A_i is an effective prefactor that includes the effect of solvent reorganization at the Pt−H_2O interface and results in time scales of 1 ns for proton-coupled electron transfers. Similarly, a prefactor corresponding to a reorganization time of 10 ns is used for the adsorption and desorption of the larger O_2 and H_2O_2 molecules on the lattice sites. Solvent reorganization time scales of 1−10 ns correspond to an additional free energy barrier of 0.22 to 0.28 eV at room temperature or an entropic barrier of 9−11 k_B if the additional barrier is entirely entropic.

The rate constants for reverse reaction steps, k_{-i}, are calculated from

$$k_{-i} = \frac{k_i}{K_i} \tag{21}$$

where K_i is the equilibrium constant. The equilibrium constant, K_i, is given by

$$K_i = \exp\left(-\frac{\Delta G_i}{k_BT}\right) \tag{22}$$

which depends on the potential through eq 14 for electrochemical steps. Kinetic parameters are summarized in Table 2 and Table 3.

Table 3. Effective Prefactor for Electrochemical Steps, A_i, and the Reaction Free Energy on Pt(111) at 0.9 V vs RHE

step	A_i/s^{-1}	$\Delta G_i^{Pt}/eV$
(3)	1.0×10^9	−0.14
(4)	1.0×10^9	−1.35
(5)	1.0×10^9	−0.05
(6)	1.0×10^9	0.15
(8)	1.0×10^9	−0.38
(9)	1.0×10^9	−0.20
(11)	1.0×10^9	0.28

Diffusion Model. In order to make direct comparisons to rotating disk electrode (RDE) experiments, which are typically used to measure electrode kinetics, we need to model O_2 diffusion to the electrode surface. In these RDE experiments, O_2 diffuses through an effective Nernstian diffusion layer of thickness, δ, while convection dominates outside the diffusion layer.

From Fick's first law, the O_2 flux is given by

$$J_{O_2} = -D_{O_2}\frac{\partial c_{O_2}}{\partial z} \tag{23}$$

where D_{O_2} is the diffusivity for O_2, c_{O_2} the concentration of O_2 and z is position away from the electrode surface. Based on Henry's law, the O_2 concentration, c_{O_2}, is given by

$$c_{O_2} = k_{H,O_2}p_{O_2} \tag{24}$$

where k_{H,O_2} is Henry's constant and p_{O_2} is the O_2 partial pressure. The O_2 mole fraction, x_{O_2}, is given by

$$x_{O_2} = \frac{c_{O_2}}{\sum_X c_X} \approx \frac{c_{O_2}}{c_{H_2O}} = \frac{k_{H,O_2}}{c_{H_2O}}p_{O_2} \tag{25}$$

If we consider the flux through a plane parallel to the surface of area A, containing one active site and 2 water molecules (cf. Figure 1) then the number of O_2 molecules diffusing through this plane is

$$\frac{\partial N_{O_2}}{\partial t} = -D_{O_2}Ac_{H_2O}\frac{\partial x_{O_2}}{\partial z} \tag{26}$$

or in terms of O_2 mole fraction

$$\frac{\partial x_{O_2}}{\partial t} = -\frac{1}{2}D_{O_2}Ac_{H_2O}\frac{\partial x_{O_2}}{\partial z} \tag{27}$$

where we have used that two water molecules are contained within the plane of area A. If we let $x_{O_2(aq)}$ and $x_{O_2(dl)}$ be the mole fraction outside the diffusion layer and at the Pt interface,

dx.doi.org/10.1021/jp4100608 | J. Phys. Chem. C 2014, 118, 6706−6718

a finite difference approximation for the O_2 concentration gradient gives

$$\frac{\partial x_{O_2}}{\partial t} = D_{O_2} A c_{H_2O} \frac{x_{O_2(aq)} - x_{O_2(dl)}}{2\delta} = k_1 x_{O_2(aq)} - k_{-1} x_{O_2(dl)} \quad (28)$$

where the latter expression shows that within our approximation, O_2 diffusion can be treated as a chemical step with rate constants

$$k_1 = k_{-1} = \frac{D_{O_2} A c_{H_2O}}{2\delta} \quad (29)$$

In this work, we simply choose a value of k_1 to match the diffusion limited current in typical rotating disk electrode experiments. We note eq 29 applies to steady state and the resulting kinetic model neglects transient concentrations of O_2 in the double layer region. However, at typical current densities and rotation speeds in RDE experiments this transient has negligible effect on the current.

Rate Equations. The described model is a set of coupled ordinary differential equations (ODEs) and the rate equations along with the site conservation conditions are given in the Supporting Information. The rate equations are solved numerically at steady state with the site conservation conditions replacing the ODEs for O_2*_A and $*_B$. The current density is calculated as

$$j = e\rho \mathrm{TOF}_{e^-} \quad (30)$$

where e is the elementary charge and ρ is the surface density of active sites and TOF_{e^-} is the turn over frequency of electrons. As one type of site takes up $^1/_3$ of the surface, $e\rho$ = 241/3 = 80.3 μC/cm^2.[37] Partial current densities for H_2O and H_2O_2 are calculated based on the expressions given by

$$j_{H_2O} = -2e\rho \mathrm{TOF}_{H_2O} \quad (31)$$

and

$$j_{H_2O_2} = -2e\rho \mathrm{TOF}_{H_2O_2} \quad (32)$$

respectively.

RESULTS

In this section, we begin by discussing the reaction mechanism of oxygen reduction on Pt(111) and we demonstrate that the developed kinetic model on Pt(111) reproduces the experimentally observed Tafel slopes and reaction order with respect to O_2. Then, employing scaling and BEP relations, we calculate the activity for O_2 reduction on metals and alloys with varying OH binding energies. We show the existence of a kinetic activity volcano and show its good agreement with the thermodynamic activity volcano. In addition, we make comparisons of the predictions of the kinetic activity volcano to a wide range of RDE experiments on Pt and Pt alloys and we find an excellent agreement between the predictions of the model and experiments.

Free Energy Diagram on Pt(111). The free energy of the different reaction intermediates on Pt(111) at 0.9 V vs RHE are listed in Table 1. The free energies of O_2*_A, $OOH*_A$ and $H_2O_2*_A$ are taken from ref 52, the free energy of $OH*_A$ is taken from ref 41. Our previous DFT calculations find oxidation of $^1/_3$ ML $OH*_A$ to $^1/_4$ M $O*$ above 0.95 V.[24] The transition between phases with different coverages is difficult to capture within the present mean-field model and we have chosen the free energy of $O*_A$ to give a reversible potential of 0.95 V for the oxidation of $^1/_3$ ML $OH*_A$ to $^1/_3$ ML $O*_A$. The free energy of $O*_B$ and $OH*_B$ are calculated in this work from the reaction energy of eq 10 and eq 12, see the Supporting Information for computational details. The free energies of $O_2(g)$ and $H_2O_2(aq)$ are obtained from the experimental reversible potentials of 1.229 and 1.776 V, respectively.[62] However, in order to represent the probability of finding an O_2 molecule at the interface, the free energy of these solvated species is expressed at a standard state with a mole fraction equal to one. Free energy diagrams for the O_2 reduction are shown in Figure 2 with free energy barriers calculated from the rate constants using eq 16.

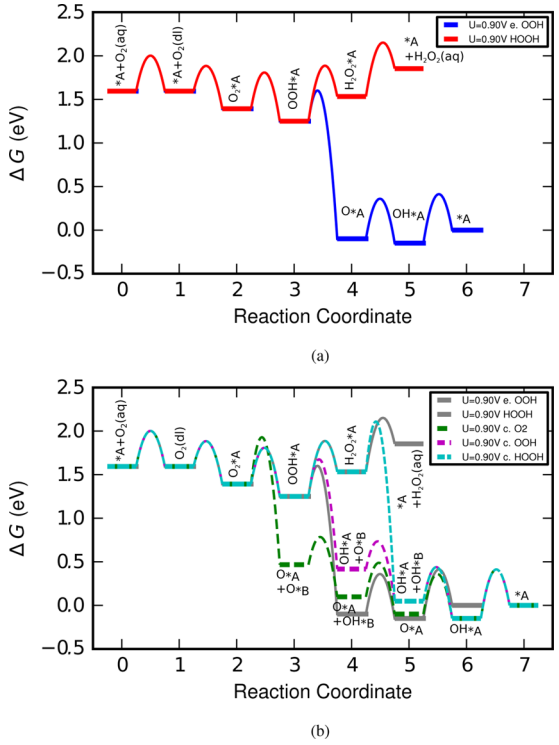

Figure 2. Free energy diagrams for O_2 reduction to H_2O and H_2O_2 on Pt(111) at 0.9 V vs RHE. (a) Shows the pathway for reduction to H_2O_2 and the dominating pathway to H_2O proceeding through electrochemical reduction of $OOH*_A$. (b) Shows minor pathways to H_2O proceeding through chemical dissociation of the O−O bond plotted on top of the pathways in part a for comparison. Only adsorbed intermediates are displayed, while protons, electrons and water have been left out for clarity.

Kinetics of ORR on Pt(111). The coverage of intermediates on Pt(111) are calculated as a function of potential and this is shown in Figure 3 for the most abundant intermediates. Above 0.95 V vs RHE the surface is dominated by $O*_A$, which is replaced by $OH*_A$ between 0.95 and 0.75 V vs RHE. Below 0.75 V vs RHE most surface sites are free. The potentials where the dominating surface species change match the corresponding equilibrium potentials in Table 1 closely, and rate analysis shows $O*_A$, $OH*_A$ and H_2O are in quasi-equilibrium at these conditions and this is consistent with previous theoretical and experimental studies.[24,37,63] The interstitial $*_B$ sites have very low intermediate coverage in the entire potential range and have been left out from Figure 3. The coverages of O_2*_A, $OOH*_A$ and $H_2O_2*_A$ are small and shown

dx.doi.org/10.1021/jp4100608 | J. Phys. Chem. C 2014, 118, 6706−6718

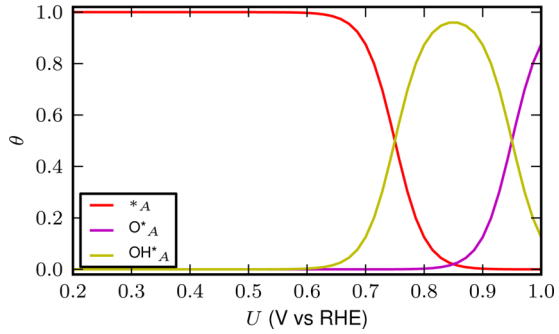

Figure 3. Simulated coverages of the most abundant adsorbates on Pt(111) as a function of electrode potential. The surface is covered by OH in the potential range 0.75−0.95 V vs RHE.

in Figure S4 in the Supporting Information together with the fraction of O_2(dl) at the catalyst-electrolyte interface. At 1.0 V vs RHE, where O_2 reduction is slow, $x_{O_2(dl)}$ equals the bulk value, $x_{O_2(aq)}$, but as the potential is lowered, O_2 is depleted from the interface and drops 2 orders of magnitude as O_2 reduction becomes diffusion limited. The corresponding total current on Pt(111) is shown as a polarization curve in Figure 4a, with an onset around 0.9 V vs RHE and a half-wave potential at 0.85 V vs RHE. We find good comparison to experimental polarization curves on Pt(111) at room temperature in 0.1 M $HClO_4$ at a rotation speed of 1600 rpm.[64,65] At lower potentials, a diffusion limited current near 6 mA/cm^2 is

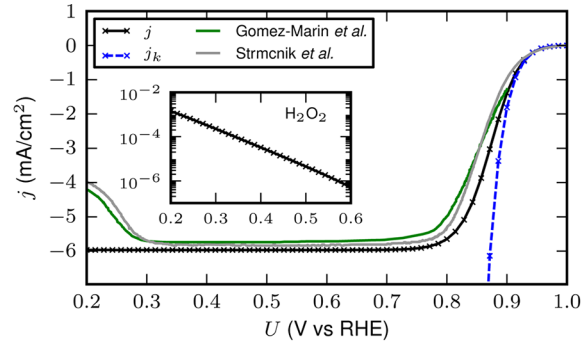

(a)

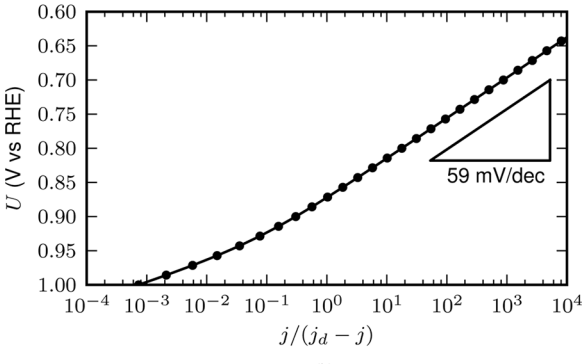

(b)

Figure 4. (a) Simulated polarization curve and kinetic current density on Pt(111) at 1600 rpm rotation speed. Experimental polarization curves on Pt(111) at room temperature in 0.1 M $HClO_4$ at a rotation speed of 1600 rpm are shown for comparison.[64,65] The inset shows the simulated partial current density for H_2O_2 at low potentials. (b) Tafel plot with a 59 mV/dec slope indicated.

reached, corresponding to a rotation speed of 1600 rpm in a RDE experiment.[9] For a diffusion limited reaction that is first order in the diffusing species, the total current, j, is related to the diffusion limited current, j_d, through

$$\frac{1}{j} = \frac{1}{j_k} + \frac{1}{j_d} \tag{33}$$

where j_k is the kinetic current that would occur in the absence of diffusion limitations. Figure 4b shows the potential plotted against

$$\frac{j}{j_d - j} = \frac{j_k}{j_d} \tag{34}$$

where j_d is taken to be the highest simulated current density. From this plot, a 59 mV/dec Tafel slope can be deduced from 0.65 to 0.9 V vs RHE, while the Tafel slope asymptotically approaches 30 mV/dec at higher potentials as O*$_A$ replaces OH*$_A$ as the dominant surface intermediate. The 59 mV/dec Tafel slope agrees with RDE experiments in $HClO_4$,[65,66] and while the Tafel slope does appear to gradually decrease at higher potentials,[65] there is no clear experimental evidence for a Tafel slope of Tafel slope of 30 mV/dec. A Tafel slope near 120 mV/dec on Pt(111) in $HClO_4$ has in some cases been reported in the diffusion limited regime,[38] however, the validity of the extrapolation to obtain the diffusion corrected kinetic current density has been questioned.[67] Our model does not reproduce a Tafel slope of 120 mV/dec.

In a RDE experiment, the Nernstian diffusion layer thickness is given by

$$\delta = 1.61 D^{1/3} \nu^{1/6} \omega^{-1/2} \tag{35}$$

where ν is the kinematic viscosity of the electrolyte and ω is the angular velocity of the RDE (in rad/s). From eq 29, it therefore follows that the rate constant of the O_2 diffusion step, eq 1, scales with rotation speed as

$$k_1 = k_1^0 \sqrt{\frac{\omega}{\omega^0}} \tag{36}$$

where ω^0 is the rotation speed of 1600 rpm and k_1^0 is the rate constant in Table 2 adjusted to give a diffusion limited current of 6 mA/cm^2 at 1600 rpm. Figure 5 shows the current density as a function of O_2 pressure at various potentials on Pt(111) and demonstrates a reaction order of 1 in agreement with RDE experiments.[65] Linearity of the Koutecky−Levich plot, is sometimes taken as evidence for a first order reaction in

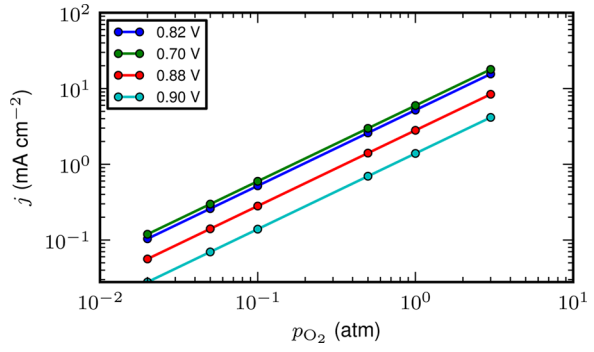

Figure 5. Current density as a function of O_2 pressure at different potentials. The reaction is seen to be first order in O_2.

dx.doi.org/10.1021/jp4100608 | J. Phys. Chem. C 2014, 118, 6706−6718

O_2,[66] and our model also reproduces this behavior as shown in Figure S5.

Trends in Activity. Using the scaling relations and BEP relations, the activity for oxygen reduction may be calculated for other catalysts as a function of their OH binding energy. Figure 6 shows the activity for O_2 reduction calculated at 0.9 V

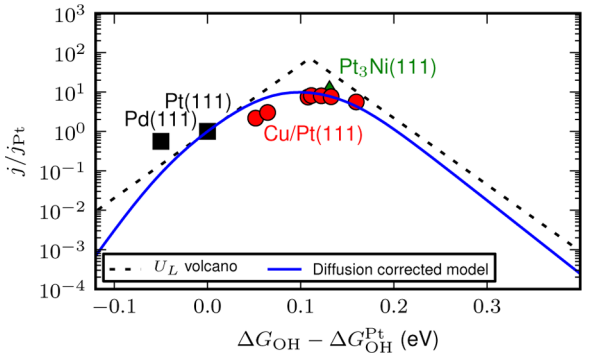

Figure 6. Simulated kinetic volcano at 0.9 V vs RHE compared to the potential limiting volcano and experiments on (111) facets. Experiments labeled Cu/Pt(111) are Pt overlayers on CuPt near surface alloys by Stephens et al..[14] The experiments for Pt(111) and $Pt_3Ni(111)$ are taken from Markovic and co-workers[21,68] and Shao et al. for Pd(111).[69]

vs RHE from the kinetic model and a thermodynamic activity volcano determined by the limiting potential is shown for comparison. The thermodynamic activity volcano for the O_2 reduction to H_2O is constructed based on the thermodynamic limiting potential for the overall reaction and the current density is normalized to that on Pt(111). The potential limiting step on the left leg of the volcano is the reduction of $OH*_A$ to H_2O while on the right leg of the volcano, it is limited by the activation of O_2 as $OOH*_A$. A more detailed discussion of this analysis can be found elsewhere.[44]

We have also made a comparison of our model for the activity to several RDE experiments on well-defined surfaces. At these conditions, the rate is significantly limited by mass transport on the most active catalysts, so the simulated current as well as the experiments on Pt(111), $Pt_3Ni(111)$ and the Cu−Pt near surface alloys have been corrected for mass transport using eq 33.

The current density for Pd(111) is calculated from the shift in the half-wave potential relative to Pt(111) and extrapolated to 0.9 V vs RHE assuming a 59 mV/dec Tafel slope.

The experimental measurements in acidic environment are all carried out in 0.1 M $HClO_4$ at a rotation speed of 1600 rpm.[14,21,68,69] The choice of $HClO_4$ is made as it is a nonadsorbing electrolyte and does not compete with the oxygen intermediates for adsorption.[63] We have intentionally avoided H_2SO_4 as bisulphate ions are known to adsorb strongly on fcc metal (111) surfaces and this could significantly affect the binding energy of oxygen intermediates, and such effects are outside the scope of the present model.[9,64]

The kinetic volcano and the thermodynamic volcano describe the same trend in activity, and the optimum activity at 0.9 V vs RHE is at a OH binding of about 0.1 eV weaker than on Pt. However, the shape of the kinetic volcano depends on potential and the maximum activity obtained from the model is lower than that from the thermodynamic volcano. The agreement with experiments is excellent in both cases.

From the results of the model, it is also possible to study trends in the $2e^-$ reduction of oxygen to H_2O_2. Figure 7

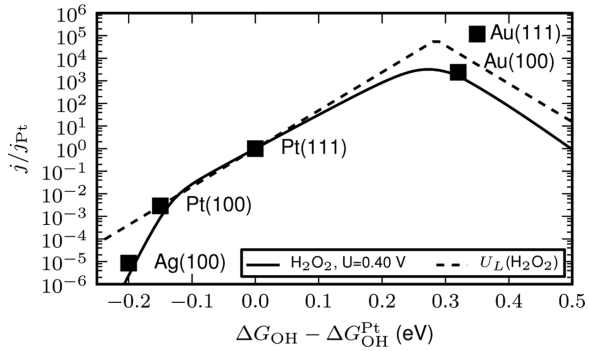

Figure 7. Simulated kinetic volcano for H_2O_2 production at 0.4 V vs RHE compared to the potential limiting volcano and experiments on (111) and (100) facets. The experiments for Pt(111) and Pt(100) are taken from Markovic and co-workers,[68] Blizanac et al. for Ag(100) and Au(100),[70,73] and Schmidt et al. for Au(111).[71]

compares the kinetic and thermodynamic volcanoes to experimental onset potentials for H_2O_2 production. The experiments on Ag(111) and Au(111) were performed in an alkaline electrolyte, 0.1 M NaOH, at rotation speeds of 1600 and 2500 rpm, respectively.[70,71] For H_2O_2 formation, the limiting potential on the left leg of the volcano is limited by the reduction of $OOH*_A$ to H_2O_2, while the right leg of the volcano is once again limited by the activation of O_2 as $OOH*_A$. A detailed discussion of this analysis can be found in our earlier work.[45] The experimental trends in H_2O_2 onset potentials are well captured by both the thermodynamic volcano and the kinetic volcano. However, O_2 reduction on Au(111) in KOH has a high selectivity toward H_2O_2 with an average of 2−3 e^- reduction of O_2,[71,72] whereas we find a lower selectivity with an average 3.5 e^- reduction of O_2 on Au(111), see Figure S6. We assign the lower selectivity for H_2O_2 production within our model to the barriers for breaking the O−O bonds being smaller than barriers compared to protonation barriers and H_2O_2 desorption.

DISCUSSION

In this section, we carry out a sensitivity analysis of the kinetic model using various rate analysis techniques. These are used to investigate the correspondence between the thermodynamic model for $2e^-$ and $4e^-$ reduction and the more detailed kinetic model.

Rate Control for H_2O Production. The most abundant reaction intermediates on the lattice $*_A$ sites are shown in Figure 8a as a function of the OH binding energy at 0.9 V vs RHE. On Pt(111), the surface is dominated by $OH*_A$. $O*_A$ coverage increases in place of $OH*_A$ on materials that bind OH stronger than Pt(111). On the weak binding side of the volcano, more free sites become available.

The degree of rate control gives the sensitivity of the reaction rate with respect to changes in a rate constant for fixed equilibrium constants. It is given by[74,75]

$$X_{\mathrm{RC},i} = \frac{k_i}{r}\left(\frac{\partial r}{\partial k_i}\right)_{k_{j\neq i},K_i} = \left(\frac{\partial[\ln r]}{\partial\left(\frac{-G_i^{\mathrm{TS}}}{k_{\mathrm{B}}T}\right)}\right)_{G_n,G_{j\neq i}^{\mathrm{TS}}} \quad (37)$$

dx.doi.org/10.1021/jp4100608 | J. Phys. Chem. C 2014, 118, 6706−6718

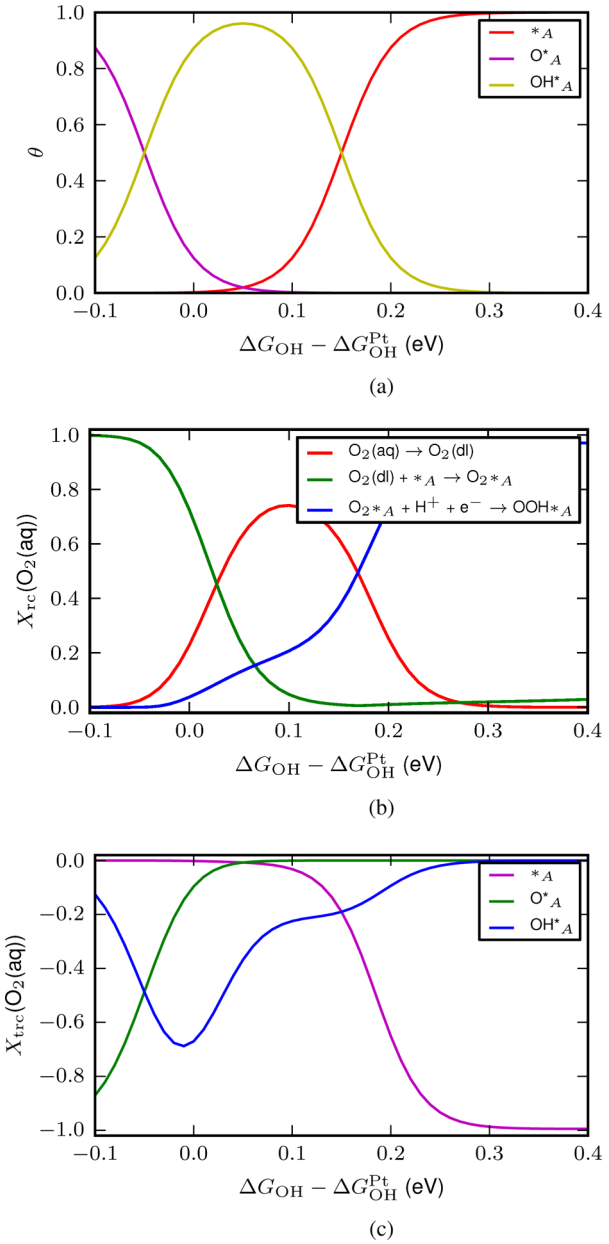

Figure 8. Most abundant reaction intermediates at 0.9 V vs RHE, (a). Degree of kinetic rate control, (b), and thermodynamic rate control, (c), of the ORR at 0.9 V vs RHE. Only degrees of rate control numerically larger than 0.01 have been shown for clarity.

where G_i^{TS} is the free energy of a transition state and G_n is the free energy of an intermediate state. The degree of rate control for O_2 reduction at 0.9 V vs RHE as a function of the free energy of OH relative to Pt(111) is shown in Figure 8b. On the strong binding side of the volcano, adsorption of O_2 from the double layer region, eq 2, has the largest degree of thermodynamic rate control, whereas the coupled proton electron transfer to O_2*_A, eq 3, has the highest degree of rate control on the weak binding side of the volcano. Near the top of the volcano the ORR is significantly limited by O_2 mass transport, and has a large contribution from eq 1 as well as eq 2 and eq 3. The degree of thermodynamic rate control describes the sensitivity of the rate to the free energy of intermediate states[75]

$$X_{\mathrm{TRC},n} = \left(\frac{\partial[\ln r]}{\partial\left(\frac{-G_n}{k_B T}\right)} \right)_{G_{m\neq n}, G_i^{TS}} \tag{38}$$

where G_n is the free energy of an intermediate state and the partial derivative is evaluated keeping the free energies of transition states and other intermediate states fixed. Such variations in G_n leads to changes in both rate constants and equilibrium constants simultaneously. The degree of thermodynamic rate control at 0.9 V vs RHE is show in Figure 8c.

On the strong binding side of the ORR volcano, $O*_A$ and $OH*_A$ have significant contributions to $X_{TRC,n}$, with $OH*_A$ being the intermediate with the numerically largest contribution to the degree of rate control on Pt(111). This reflects the fact that Pt(111) binds OH too strongly and destabilizing OH would lead to an improved rate on Pt(111). On materials that bind OH weaker relative to Pt(111), the degree of thermodynamic rate control of $OH*_A$ decreases numerically. On the weak binding side of the volcano, the free energy of vacant sites obtains the numerically largest degree of rate control. This reflects the fact that intermediates on the weak binding side of the volcano are too unstable and decreasing the stability of vacant sites will increase the coverage of O_2*_A which precedes the rate-determining step eq 3. The degree of rate control and degree of thermodynamic rate control describes the effect of changing the free energy of a single transition state or intermediate while keeping all other energies constant. Because of BEP and scaling relations, these free energies are highly correlated and improving the rate of the rate-determining step does not improve the rate on Pt(111) because the reaction is also limited thermodynamically by removal of $OH*_A$. This insight is captured in the empirically derived expression by Markovic and Ross who have emphasized the importance of destabilizing OH.[2] The difficulties associated with activation of the O_2 molecule on the weak binding side of the volcano was also found in recent DFT studies by Mavrikakis and co-workers and Anderson and co-workers.[76,77]

Sabatier Volcano. In this section, we perform a Sabatier analysis,[78] in order to derive simplified rate expressions at 0.9 V vs RHE that hold when a single step is rate determining in the absence of mass transport limitations. On the basis of rate control analysis, we suggest that the turn over frequency of O_2 reduction on the weak binding leg is well described by the activation of O_2 given by

$$\mathrm{TOF}_{O_2,w} = k_3 \theta_{O_2*_A} = k_3 K_2 x_{O_2(aq)} \tag{39}$$

We suggest that the turn over frequency of O_2 reduction on the strong binding side of the volcano is controlled by the coverage of free sites. This is given by

$$\mathrm{TOF}_{O_2,s} = k_2^0 x_{O_2(aq)} \theta_{*A} \tag{40}$$

where k_2^0 is the rate constant for O_2 adsorption at not too weak binding of O_2*_A such that k_2^0 is material independent, and $\theta*_A$ is the coverage of free sites. According to our rate control analysis and De Donder analysis,[79,80] $O*_A$ and $OH*_A$ are the primary species blocking the active sites and their coverage should be well-determined by quasi equilibrium with H_2O. Consequently, the coverage of free sites may be approximated by an effective Langmuir isotherm

dx.doi.org/10.1021/jp4100608 | J. Phys. Chem. C 2014, 118, 6706−6718

$$\theta_{*_A} = 1 - \theta_{OH*_A} - \theta_{O*_A} = \frac{1}{1 + K_6^{-1} + K_5^{-1}K_6^{-1}} = \frac{K_5K_6}{1 + K_5 + K_5K_6} \quad (41)$$

The $4e^-$ reduction of O_2 dominates at these conditions and thus, the current density is given by

$$j = -4\rho e \mathrm{TOF}_{O_2} \quad (42)$$

The current described by the rate equations for $\mathrm{TOF}_{O_2,w}$ and $\mathrm{TOF}_{O_2,s}$ is shown in Figure 9 together with the full kinetic

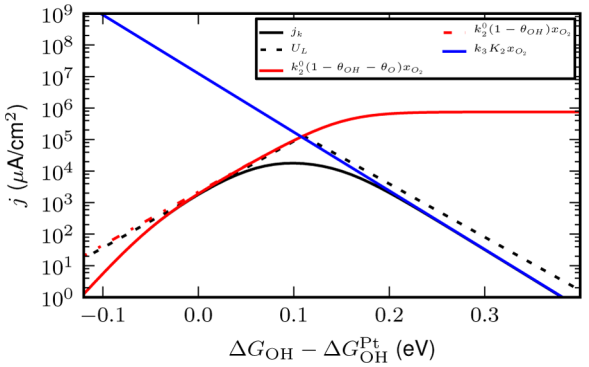

Figure 9. Plot of the activity volcano for the full kinetic model and that derived using a simplified Sabatier analysis. The volcano using the potential limiting analysis is shown for comparison. Mass transport limitations have been removed from the full kinetic model and also neglected in the Sabatier analysis. The potential limiting volcano is normalized to the kinetic current density on Pt(111) in the full model.

model corrected for mass transport limitations. The full kinetic model approaches $\mathrm{TOF}_{O_2,s}$ and $\mathrm{TOF}_{O_2,w}$ asymptotically at strong and weak binding respectively confirming our rate analysis. The Sabatier rate is given by the minimum of the asymptotic rates

$$\mathrm{TOF}_{O_2,\mathrm{Sabatier}} = \min(\mathrm{TOF}_{O_2,s}, \mathrm{TOF}_{O_2,w}) \quad (43)$$

and is an upper bound for the rate of the full model. The Sabatier rate approaches the rate of the full model on both sides of the volcano, where the rate is well described by a single rate-determining step, but overpredicts the rate near the top of the volcano where a single step is not rate determining. The Sabatier volcano also agrees well with the potential limiting volcano.

Correspondence between Kinetic and Thermodynamic Volcanoes. The correspondence between the Sabatier volcano and the potential limiting volcano is excellent on the strong binding leg. At OH binding, slightly stronger than Pt(111), there is a deviation between the potential limiting volcano and the Sabatier volcano, caused by $O*_A$ blocking the surface instead of $OH*_A$. Thus, in the Sabatier model $O*_A$ removal limits the rate at this potential whereas removal of $OH*_A$ is potential limiting. If the available free sites is calculated from OH adsorption alone

$$\theta_{*_A} = 1 - \theta_{OH*_A} = \frac{1}{1 + K_6^{-1}} = \frac{K_6}{1 + K_6} \quad (44)$$

the Sabatier volcano and the potential limiting volcano becomes equivalent in the strong binding region as shown in Figure 9. The origin of the agreement between the weak binding legs of the two volcanoes is less obvious, since both the agreement between the slope and the position of the weak binding leg relative to the Pt(111) need to be explained. The slope of the weak binding leg of the Sabatier volcano is given by the variation of k_3K_2 with OH binding, which expresses the change in the transition state energy for the electrochemical reduction of O_2*_A to $OOH*_A$. Because of the scaling between O_2*_A and $OOH*_A$, this variation follows the scaling of $OOH*_A$ closely, and OOH also determines the slope of the potential limiting volcano. The position of the weak binding leg relative to Pt(111) is given by the ratio

$$\frac{\mathrm{TOF}_{O_2,w}}{\mathrm{TOF}_{O_2,s}} = \frac{k_3K_2}{k_2^0}\frac{1}{\theta_{*_A}} \quad (45)$$

whereas the corresponding quantity for the potential limiting volcano is determined by the limiting potentials for OH removal and OOH formation on Pt(111). Here OH removal corresponds to the $1/(\theta_{*_A})$ term, while OOH activation corresponds to the ratio $(k_3K_2)/(k_2^0)$, which turns out to be rather small.

A critical component in reproducing the reaction order with respect to O_2 on Pt(111) is the slow adsorption of O_2, which is caused by the low O_2 mole fraction at the interface (x_{O_2}) and the slow time scale for solvent reorganization at the interface (k_2^0). It can be seen from eq 45 that in describing the rate relative to Pt(111), x_{O_2} cancels out, while there is a high degree of cancellation of the time scale for solvent reorganization present in both k_3 and k_2^0. This demonstrates that while a kinetic parameter may be crucial in understanding the reaction mechanism on one material, it could be largely irrelevant for understanding trends in activity. The sensitivity of the kinetic volcano to variations in time scales of solvent reorganization is shown in Figure S7.

We note that eq 41 provides an easy interpretation of the Tafel slopes and reaction order with respect to O_2 on Pt(111). The only potential dependent term in eq 41 is the coverage of free sites, θ_{*_A}, which gives rise to a 59 mV/dec Tafel slope when the OH adsorption dominates the surface and $\theta_{*_A} \approx 1 - \theta_{OH*_A} \ll 1$, and a 30 mV/dec Tafel slope when O adsorption dominates the surface $\theta_{*_A} \approx 1 - \theta_{O*_A} \ll 1$. The reaction order with respect to O_2 is one because x_{O_2} is linear in O_2 pressure.

Rate Control for H_2O_2 Production. Our sensitivity analysis of H_2O_2 production in Figure 10 shows that the selectivity for H_2O_2 is sensitive to most kinetic parameters. For example, Pt(111) has $X_{RC,13} = 1$ for H_2O_2 desorption, eq 13, and $X_{RC,12} = -1$ for H_2O_2 dissociation, eq 12. As OH binding is weakened relative to Pt, both degrees of rate control tend to zero at the same rate. Similar behavior is observed for O_2 dissociation, eq 7, and OOH formation, eq 3, for materials that bind OH 0.1 eV stronger than Pt, where O_2 dissociation is a significant pathway toward H_2O. OOH reduction to O, eq 4, is mirrored by OOH reduction to H_2O_2, eq 11, for materials that bind OH weaker than Pt(111), while chemical OOH dissociation, eq 4, becomes a more important pathway than OOH reduction to O that reduces the selectivity for H_2O_2 for materials that bind OH 0.2 eV weaker than Pt(111). In addition to the above steps that branch between H_2O_2 and H_2O, the

dx.doi.org/10.1021/jp4100608 | J. Phys. Chem. C 2014, 118, 6706−6718

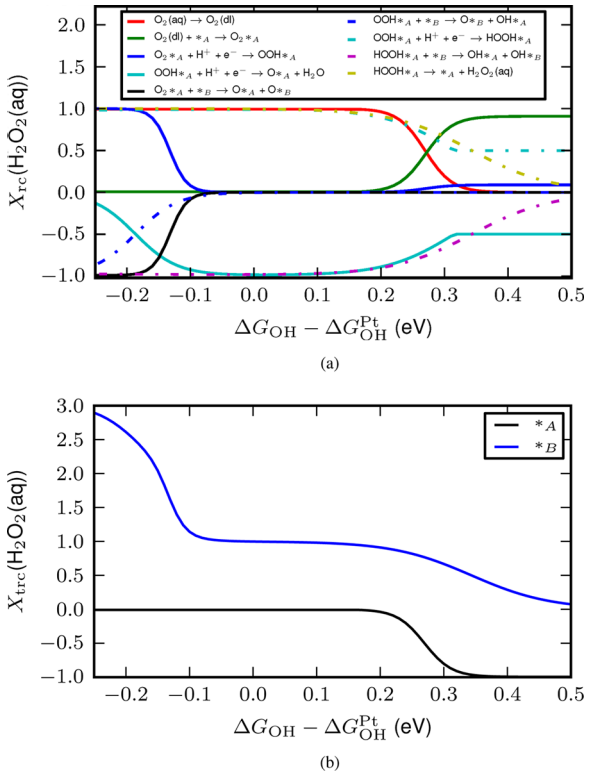

Figure 10. Degree of kinetic rate control (a) and thermodynamic rate control (b) of the $2e^-$ reduction of O_2 to H_2O_2 at 0.4 V vs RHE. Only degrees of rate control numerically larger than 0.01 have been shown for clarity.

H_2O_2 rate is controlled by O_2 diffusion for materials that binds OH stronger than 0.3 eV vs OH on Pt(111) while O_2 adsorption and OOH formation control the rate on materials that bind OH weaker than about 0.2 eV on Pt(111). We note that all steps that break the O−O bond are irreversible. At 0.4 V vs RHE both the lattice sites and the interstitial sites are free of adsorbates within our model. Consequently, free sites are the only surface species with significant thermodynamic rate control as shown in Figure 10b. At weak OH binding, $*_A$ has a negative degree of thermodynamic rate control, as stabilizing all adsorbed species would improve the rate of H_2O_2 and H_2O production. The positive degree of thermodynamic rate control for $*_B$ is due to the fact that stabilization of $*_B$ leads to smaller rate constants for the chemical O−O scission steps in eq 7, eq 10 and eq 12, as the free energy of the initial state is increased while the free energy of the transition state is constant according to eq 38. For OH binding energies 0.1 eV stronger than Pt(111), the dominant mechanism for O−O scission shifts from electrochemical $OOH*_A$ reduction, eq 4, to O_2 dissociation, eq 7, which increases the sensitivity to the $*_B$ energy for materials that bind OH 0.1 eV stronger than Pt(111) due to an earlier branching between the H_2O and H_2O_2 pathways.

Model Limitations. The kinetic model developed in this work is based on DFT calculations of the solvated H_2O−OH interface, where H_2O at the interface stabilizes reaction intermediates through hydrogen bonding. Reaction intermediates are sufficiently separated in the hydrogen bonding network with H_2O that adsorbate−adsorbate interactions such as the $OH*_A$−$OH*_A$ interaction can be expected to be small.[52] However, at higher potentials or on materials that bind intermediates much stronger than Pt(111), O* coverage may be higher than the saturation coverage of $^1/_3$ ML assumed in this model. At these conditions, repulsive O*−O* interactions and changes in the solvation of OH and OOH correlated to O* formation are expected to become important.[24] However, these effects have not been investigated in detail within the present model. We would like to point out that the model has been limited to nonadsorbing electrolytes. The well-known effect of the specific adsorption of anions such as bisulphate or cyanide from the electrolyte in RDE experiments[9,64] has not been considered and these block active sites in addition to modifying adsorbate binding energies through adsorbate−adsorbate interactions. The kinetic and thermodynamic parameters are calculated on extended (111) facets and further experimental and theoretical work would be needed to extend the kinetic model to extended stepped surfaces, where, e.g., the solvation and structure of the important OH intermediate is still not well understood.[55,81]

The reaction mechanism assumes an acid electrolyte and neglects in particular the possible adsorption of O_2^- from solution, which has been proposed to be important for e.g. ORR on Ag(111) in alkaline.[70] Additionally, the calculated proton transfer barrier of ref 52 is based on a solvated proton while the barrier for the transfer of a proton from H_2O in alkaline may be different, which may affect the relative preference for electrochemical and chemical steps within the framework of eq 20. The important role played by pH in determining the ORR kinetics requires a more detailed investigation and is outside the scope of the present work.

CONCLUSION

In this work, we have developed a microkinetic model for oxygen reduction based on density functional theory calculations. The developed model reproduces kinetic parameters consistent with experiments on Pt(111). On the basis of scaling and BEP relations, we further demonstrate the existence of a kinetic activity volcano and show its close connection to the thermodynamic activity volcano. Both of these analysis identify an activity optimum at 0.1 eV weaker OH binding than Pt(111). For strong binding surfaces such as Pt(111), the removal of OH* is the potential limiting step in the thermodynamic model, while in the kinetic model, OH removal has thermodynamic rate control but is not the rate limiting step. For weak binding surfaces, OOH formation has high degree of rate control in the kinetic model and is the potential limiting step in the thermodynamic model. The predictions of the kinetic activity volcano compare well with a wide range of RDE experiments on metals and Pt alloys. We also use the developed model to analyze the $2e^-$ reduction of oxygen and show the correspondence between the kinetic and thermodynamic activity volcano for the H_2O_2 production. Both analyses identify an activity optimum at around 0.3 eV weaker binding of OH than Pt(111). On the basis of rate control analysis, we show that several steps play a key role in determining the selectivity and such detailed microkinetic analysis is necessary for addressing trends in selectivity.

ASSOCIATED CONTENT

Supporting Information

Rate equations, BEP relations and scaling relations used in the kinetic model, plots of the most abundant reaction intermediates, the effect of O_2 pressure, and the average number of electrons transferred as a function of OH binding

dx.doi.org/10.1021/jp4100608 | J. Phys. Chem. C 2014, 118, 6706−6718

energy. This material is available free of charge via the Internet at http://pubs.acs.org.

AUTHOR INFORMATION

Corresponding Authors

*E-mail: hahansen@stanford.edu.
*E-mail: norskov@stanford.edu.

Notes

The authors declare no competing financial interest.

ACKNOWLEDGMENTS

The authors acknowledge support from the Department of Energy, Basic Energy Sciences, through the SUNCAT Center for Interface Science and Catalysis.

REFERENCES

(1) Marković, N. M.; Schmidt, T. J.; Stamenkovic, V.; Ross, P. N. Oxygen Reduction Reaction on Pt and Pt Bimetallic Surfaces: A Selective Review. *Fuel Cells* **2001**, *1*, 105−116.

(2) Marković, N. M.; Ross, P. N. Surface Science Studies of Model Fuel Cell Electrocatalysts. *Surf. Sci. Rep.* **2002**, *45*, 117−229.

(3) Mukerjee, S.; Srinivasan, S.; Soriaga, M. P.; McBreen, J. Role of Structural and Electronic Properties of Pt and Pt Alloys on Electrocatalysis of Oxygen Reduction An in situ XANES and EXAFS Investigation. *J. Electrochem. Soc.* **1995**, *142*, 1409−1422.

(4) Marković, N. M.; Gasteiger, H. A.; Ross, P. N. Oxygen Reduction on Platinum Low-Index Single-Crystal Surfaces in Sulfuric Acid Solution: Rotating Ring-Pt(hkl) Disk Studies. *J. Phys. Chem.* **1995**, *99*, 3411−3415.

(5) Stamenkovic, V.; M. Marković, N.; Ross, P. Structure-Relationships in Electrocatalysis: Oxygen Reduction and Hydrogen Oxidation Reactions on Pt(111) and Pt(100) in Solutions Containing Chloride Ions. *J. Electroanal. Chem.* **2001**, *500*, 44−51.

(6) Zhang, J.; Vukmirovic, M. B.; Xu, Y.; Mavrikakis, M.; Adzic, R. R. Controlling the Catalytic Activity of Platinum-Monolayer Electrocatalysts for Oxygen Reduction with Different Substrates. *Angew. Chem., Int. Ed.* **2005**, *44*, 2132−2135.

(7) Climent, V.; Gomez, R.; Orts, J. M.; Feliu, J. M. Thermodynamic Analysis of the Temperature Dependence of OH Adsorption on Pt(111) and Pt(100) Electrodes in Acidic Media in the Absence of Specific Anion Adsorption. *J. Phys. Chem. B* **2006**, *110*, 11344−11351.

(8) Zhou, W.-P.; Yang, X.; Vukmirovic, M. B.; Koel, B. E.; Jiao, J.; Peng, G.; Mavrikakis, M.; Adzic, R. R. Improving Electrocatalysts for O_2 Reduction by Fine-Tuning the Pt-Support Interaction: Pt Monolayer on the Surfaces of a $Pd_3Fe(111)$ Single-Crystal Alloy. *J. Am. Chem. Soc.* **2009**, *131*, 12755−12762.

(9) Kuzume, A.; Herrero, E.; Feliu, J. M. Oxygen Reduction on Stepped Platinum Surfaces in Acidic Media. *J. Electroanal. Chem.* **2007**, *599*, 333−343.

(10) Macia, M.; Campina, J.; Herrero, E.; Feliu, J. M. On the Kinetics of Oxygen Reduction on Platinum Stepped Surfaces in Acidic Media. *J. Electroanal. Chem.* **2004**, *564*, 141−150.

(11) Wakisaka, M.; Suzuki, H.; Mitsui, S.; Uchida, H.; Watanabe, M. Identification and Quantification of Oxygen Species Adsorbed on Pt(111) Single-Crystal and Polycrystalline Pt Electrodes by Photoelectron Spectroscopy. *Langmuir* **2009**, *25*, 1897−1900.

(12) Wakisaka, M.; Udagawa, Y.; Suzuki, H.; Uchida, H.; Watanabe, M. Structural Effects on the Surface Oxidation Processes at Pt Single-Crystal Electrodes Studied by X-Ray Photoelectron Spectroscopy. *Energ. Environ. Sci.* **2011**, *4*, 1662−1666.

(13) Kondo, S.; Nakamura, M.; Maki, N.; Hoshi, N. Active Sites for the Oxygen Reduction Reaction on the Low and High Index Planes of Palladium. *J. Phys. Chem. C* **2009**, *113*, 12625−12628.

(14) Stephens, I. E. L.; Bondarenko, A. S.; Perez-Alonso, F. J.; Calle-Vallejo, F.; Bech, L.; Johansson, T. P.; Jepsen, A. K.; Frydendal, R.; Knudsen, B. P.; Rossmeisl, J.; Chorkendorff, I. Tuning the Activity of Pt(111) for Oxygen Electroreduction by Subsurface Alloying. *J. Am. Chem. Soc.* **2011**, *133*, 5485−5491.

(15) Damjanovic, A.; Genshaw, M.; Bockris, J. The Mechanism of Oxygen Reduction at Platinum in Alkaline Solutions with Special Reference to H_2O_2. *J. Electrochem. Soc.* **1967**, *114*, 1107−1112.

(16) Fernández, J. L.; Bard, A. J. Scanning Electrochemical Microscopy. 47. Imaging Electrocatalytic Activity for Oxygen Reduction in an Acidic Medium by the Tip Generation-Substrate Collection Mode. *Anal. Chem.* **2003**, *75*, 2967−2974.

(17) Hoster, H.; Richter, B.; Behm, R. J. Catalytic Influence of Pt Monolayer Islands on the Hydrogen Electrochemistry of Ru(0001) Studied by Ultrahigh Vacuum Scanning Tunneling Microscopy and Cyclic Voltammetry. *J. Phys. Chem. B* **2004**, *108*, 14780−14788.

(18) Maillard, F.; Lu, G.-Q.; Wieckowski, A.; Stimming, U. Ru-Decorated Pt Surfaces as Model Fuel Cell Electrocatalysts for CO Electrooxidation. *J. Phys. Chem. B* **2005**, *109*, 16230−16243.

(19) Fernández, J. L.; Walsh, D. A.; Bard, A. J. Thermodynamic Guidelines for the Design of Bimetallic Catalysts for Oxygen Electroreduction and Rapid Screening by Scanning Electrochemical Microscopy. M-Co (M: Pd, Ag, Au). *J. Am. Chem. Soc.* **2005**, *127*, 357−365.

(20) Rosca, V.; Koper, M. T. M. Electrocatalytic Oxidation of Ammonia on Pt(111) and Pt(100) Surfaces. *Phys. Chem. Chem. Phys.* **2006**, *8*, 2513−2524.

(21) Stamenkovic, V. R.; Fowler, B.; Mun, B. S.; Wang, G. F.; Ross, P. N.; Lucas, C. A.; Marković, N. M. Improved Oxygen Reduction Activity on $Pt_3Ni(111)$ via Increased Surface Site Availability. *Science* **2007**, *315*, 493−497.

(22) Anderson, A. B. O_2 Reduction and CO Oxidation at the Pt-Electrolyte Interface: The role of H_2O and OH Adsorption Bond Strengths. *Electrochim. Acta* **2002**, *47*, 3759−3763.

(23) Anderson, A. B.; Sidik, R. A.; Narayanasamy, J.; Shiller, P. Theoretical Calculation of Activation Energies for $Pt + H^+(aq) + e^-(U) \leftrightarrow Pt - H$: Activation Energy-Based Symmetry Factors in the Marcus Normal and Inverted Regions. *J. Phys. Chem. B* **2003**, *107*, 4618−4623.

(24) Viswanathan, V.; Hansen, H. A.; Rossmeisl, J.; Jaramillo, T. F.; Pitsch, H.; Nørskov, J. K. Simulating Linear Sweep Voltammetry from First-Principles: Application to Electrochemical Oxidation of Water on Pt(111) and $Pt_3Ni(111)$. *J. Phys. Chem. C* **2012**, *116*, 4698−4704.

(25) Gohda, Y.; Schnur, S.; Groß, A. Influence of Water on Elementary Reaction Steps in Electrocatalysis. *Faraday Discuss.* **2009**, *140*, 233−244.

(26) Janik, M. J.; Taylor, C. D.; Neurock, M. First-Principles Analysis of the Initial Electroreduction Steps of Oxygen over Pt(111). *J. Electrochem. Soc.* **2009**, *156*, B126−B135.

(27) Anderson, A. B.; Uddin, J.; Jinnouchi, R. Solvation and Zero-Point-Energy Effects on OH(ads) Reduction on Pt(111) Electrodes. *J. Phys. Chem. C* **2010**, *114*, 14946−14952.

(28) Jinnouchi, R.; Hatanaka, T.; Morimoto, Y.; Osawa, M. First Principles Study of Sulfuric Acid Anion Adsorption on a Pt(111) Electrode. *Phys. Chem. Chem. Phys.* **2012**, *14*, 3208−3218.

(29) Keith, J. A.; Jacob, T. Theoretical Studies of Potential-Dependent and Competing Mechanisms of the Electrocatalytic Oxygen Reduction Reaction on Pt(111). *Angew. Chem., Int. Ed.* **2010**, *49*, 9521−9525.

(30) Nilekar, A. U.; Mavrikakis, M. Improved Oxygen Reduction Reactivity of Platinum Monolayers on Transition Metal Surfaces. *Surf. Sci.* **2008**, *602*, L89−L94.

(31) Sha, Y.; Yu, T. H.; Merinov, B. V.; Shirvanian, P.; Goddard, W. A. Mechanism for Oxygen Reduction Reaction on Pt_3Ni Alloy Fuel Cell Cathode. *J. Phys. Chem. C* **2012**, *116*, 21334−21342.

(32) Lee, S. W.; Chen, S.; Suntivich, J.; Sasaki, K.; Adzic, R. R.; Shao-Horn, Y. Role of Surface Steps of Pt Nanoparticles on the Electrochemical Activity for Oxygen Reduction. *J. Phys. Chem. Lett.* **2010**, *1*, 1316−1320.

(33) Shao, M.; Peles, A.; Shoemaker, K. Electrocatalysis on Platinum Nanoparticles: Particle Size Effect on Oxygen Reduction Reaction Activity. *Nano Lett.* **2011**, *11*, 3714−3719.

(34) Leontyev, I. N.; Belenov, S. V.; Guterman, V. E.; Haghi-Ashtiani, P.; Shaganov, A. P.; Dkhil, B. Catalytic Activity of Carbon-Supported Pt Nanoelectrocatalysts. Why Reducing the Size of Pt Nanoparticles is Not Always Beneficial. *J. Phys. Chem. C* **2011**, *115*, 5429−5434.
(35) Viswanathan, V.; Wang, F. Y. F. Theoretical Analysis of the Effect of Particle Size and Support on the Kinetics of Oxygen Reduction Reaction on Platinum Nanoparticles. *Nanoscale* **2012**, *4*, 5110−5117.
(36) Perez-Alonso, F. J.; McCarthy, D. N.; Nierhoff, A.; Hernandez-Fernandez, P.; Strebel, C.; Stephens, I. E. L.; Nielsen, J. H.; Chorkendorff, I. The Effect of Size on the Oxygen Electroreduction Activity of Mass-Selected Platinum Nanoparticles. *Angew. Chem., Int. Ed.* **2012**, *51*, 4641−4643.
(37) Wang, J. X.; Marković, N. M.; Adzic, R. R. Kinetic Analysis of Oxygen Reduction on Pt(111) in Acid Solutions: Intrinsic Kinetic Parameters and Anion Adsorption Effects. *J. Phys. Chem. B* **2004**, *108*, 4127−4133.
(38) Wang, J. X.; Zhang, J.; Adzic, R. R. Double-Trap Kinetic Equation for the Oxygen Reduction Reaction on Pt(111) in Acidic Media. *J. Phys. Chem. A* **2007**, *111*, 12702−12710.
(39) Marković, N. M.; Gasteiger, H. A.; Grgur, B. N.; Ross, P. N. Oxygen Reduction Reaction on Pt(111): Effects of Bromide. *J. Electroanal. Chem.* **1999**, *467*, 157−163.
(40) Nørskov, J. K.; Rossmeisl, J.; Logadottir, A.; Lindqvist, L.; Kitchin, J. R.; Bligaard, T.; Jonsson, H. Origin of the Overpotential for Oxygen Reduction at a Fuel-Cell Cathode. *J. Phys. Chem. B* **2004**, *108*, 17886−17892.
(41) Karlberg, G. S.; Rossmeisl, J.; Nørskov, J. K. Estimations of Electric Field Effects on the Oxygen Reduction Reaction Based on the Density Functional Theory. *Phys. Chem. Chem. Phys.* **2007**, *9*, 5158−5161.
(42) Greeley, J.; Stephens, I. E. L.; Bondarenko, A. S.; Johansson, T. P.; Hansen, H. A.; Jaramillo, T. F.; Rossmeisl, J.; Chorkendorff, I.; Nørskov, J. K. Alloys of Platinum and Early Transition Metals as Oxygen Reduction Electrocatalysts. *Nat. Chem.* **2009**, *1*, 552−556.
(43) Abild-Pedersen, F.; Greeley, J.; Studt, F.; Rossmeisl, J.; Munter, T. R.; Moses, P. G.; Skulason, E.; Bligaard, T.; Nørskov, J. K. Scaling Properties of Adsorption Energies for Hydrogen-Containing Molecules on Transition-Metal Surfaces. *Phys. Rev. Lett.* **2007**, *99*, 016105.
(44) Viswanathan, V.; Hansen, H. A.; Rossmeisl, J.; Nørskov, J. K. Universality in Oxygen Reduction Electrocatalysis on Metal Surfaces. *ACS Catal.* **2012**, *2*, 1654−1660.
(45) Viswanathan, V.; Hansen, H. A.; Rossmeisl, J.; Nørskov, J. K. Unifying the $2e^-$ and $4e^-$ Reduction of Oxygen on Metal Surfaces. *J. Phys. Chem. Lett.* **2012**, *3*, 2948−2951.
(46) Nørskov, J. K.; Bligaard, T.; Logadottir, A.; Kitchin, J. R.; Chen, J. G.; Pandelov, S.; Stimming, U. Trends in the Exchange Current for Hydrogen Evolution. *J. Electrochem. Soc.* **2005**, *152*, 23−26.
(47) Man, I.; Su, H.; Calle-Vallejo, F.; Hansen, H.; Martnez, J.; Inoglu, N.; Kitchin, J.; Jaramillo, T.; Nørskov, J.; Rossmeisl, J. Universality in Oxygen Evolution Electrocatalysis on Oxide Surfaces. *ChemCatChem* **2011**, *3*, 1159−1165.
(48) Hansen, H. A.; Varley, J. B.; Peterson, A. A.; Nørskov, J. K. Understanding Trends in the Electrocatalytic Activity of Metals and Enzymes for CO_2 Reduction to CO. *J. Phys. Chem. Lett.* **2013**, *4*, 388−392.
(49) Greeley, J.; Jaramillo, T. F.; Bonde, J.; Chorkendorff, I. B.; Nørskov, J. K. Computational High-Throughput Screening of Electrocatalytic Materials for Hydrogen Evolution. *Nat. Mater.* **2006**, *5*, 909−913.
(50) Rossmeisl, J.; Karlberg, G. S.; Jaramillo, T.; Nørskov, J. K. Steady State Oxygen Reduction and Cyclic Voltammetry. *Faraday Discuss.* **2009**, *140*, 337−346.
(51) Rossmeisl, J.; Nørskov, J. K.; Taylor, C. D.; Janik, M. J.; Neurock, M. Calculated Phase Diagrams for the Electrochemical Oxidation and Reduction of Water over Pt(111). *J. Phys. Chem. B* **2006**, *110*, 21833−21839.
(52) Tripkovic, V.; Skúlason, E.; Siahrostami, S.; Nørskov, J. K.; Rossmeisl, J. The Oxygen Reduction Reaction Mechanism on Pt(111) from Density Functional Theory Calculations. *Electrochim. Acta* **2010**, *55*, 7975−7981.
(53) Karlberg, G. S.; Wahnström, G. An Interaction Model for OH $+H_2O$-Mixed and Pure H_2O Overlayers Adsorbed on Pt(111). *J. Chem. Phys.* **2005**, *122*, 194705.
(54) Xu, Y.; Ruban, A. V.; Mavrikakis, M. Adsorption and Dissociation of O_2 on Pt-Co and Pt-Fe Alloys. *J. Am. Chem. Soc.* **2004**, *126*, 4717−4725.
(55) Stephens, I. E. L.; Bondarenko, A. S.; Grønbjerg, U.; Rossmeisl, J.; Chorkendorff, I. Understanding the Electrocatalysis of Oxygen Reduction on Platinum and its Alloys. *Energ. Environ. Sci.* **2012**, *5*, 6744−6762.
(56) Grabow, L. C.; Hvolbæk, B.; Falsig, H.; Nørskov, J. K. Search Directions for Direct H_2O_2 Synthesis Catalysts Starting from Au_{12} Nanoclusters. *Top. Catal.* **2012**, *55*, 336−344.
(57) Ford, D. C.; Nilekar, A. U.; Xu, Y.; Mavrikakis, M. Partial and Complete Reduction of O_2 by Hydrogen on Transition Metal Surfaces. *Surf. Sci.* **2010**, *604*, 1565−1575.
(58) Rankin, R. B.; Greeley, J. Trends in Selective Hydrogen Peroxide Production on Transition Metal Surfaces from First Principles. *ACS Catal.* **2012**, *2*, 2664−2672.
(59) Rossmeisl, J.; Logadottir, A.; Nørskov, J. K. Electrolysis of Water on (Oxidized) Metal Surfaces. *Chem. Phys.* **2005**, *319*, 178−184.
(60) Jinnouchi, R.; Kodama, K.; Hatanaka, T.; Morimoto, Y. First Principles Based Mean Field Model for Oxygen Reduction Reaction. *Phys. Chem. Chem. Phys.* **2011**, *13*, 21070−21083.
(61) Limmer, D. T.; Willard, A. P.; Madden, P.; Chandler, D. Hydration of Metal Surfaces can be Dynamically Heterogeneous and Hydrophobic. *Proc. Natl. Acad. Sci. U.S.A.* **2013**, *110*, 4200−4205.
(62) Haynes, W. M.; Bruno, T. J.; Lide, D. R. *CRC Handbook of Chemistry and Physics*, 93rd ed.; CRC Press/Taylor and Francis: Boca Raton, FL, 2013.
(63) Bondarenko, A. S.; Stephens, I. E. L.; Hansen, H. A.; Pérez-Alonso, F. J.; Tripkovic, V.; Johansson, T. P.; Rossmeisl, J.; Nørskov, J. K.; Chorkendorff, I. The Pt(111)/Electrolyte Interface under Oxygen Reduction Reaction Conditions: An Electrochemical Impedance Spectroscopy Study. *Langmuir* **2011**, *27*, 2058−2066.
(64) Strmcnik, D.; Escudero-Escribano, M.; Kodama, K.; Stamenkovic, V. R.; Cuesta, A.; Marković, N. M. Enhanced Electrocatalysis of the Oxygen Reduction Reaction Based on Patterning of Platinum Surfaces with Cyanide. *Nat. Chem.* **2010**, *2*, 880−885.
(65) Gómez-Marn, A. M.; Feliu, J. M. New Insights into the Oxygen Reduction Reaction Mechanism on Pt (111): A Detailed Electrochemical Study. *ChemSusChem* **2013**, *6*, 1091−1100.
(66) Marković, N. M.; Adžić, R. R.; Cahan, B. D.; Yeager, E. B. Structural Effects in Electrocatalysis: Oxygen Reduction on Platinum Low Index Single-Crystal Surfaces in Perchloric Acid Solutions. *J. Electroanal. Chem.* **1994**, *377*, 249−259.
(67) Neyerlin, K. C.; Gu, W.; Jorne, J.; Gasteiger, H. A. Determination of Catalyst Unique Parameters for the Oxygen Reduction Reaction in a PEMFC. *J. Electrochem. Soc.* **2006**, *153*, A1955−A1963.
(68) Marković, N. M.; Gasteiger, H. A.; Ross, P. N. Kinetics of Oxygen Reduction on Pt(hkl) Electrodes: Implications for the Crystallite Size Effect with Supported Pt Electrocatalysts. *J. Electrochem. Soc.* **1997**, *144*, 1591−1597.
(69) Shao, M. H.; Huang, T.; Liu, P.; Zhang, J.; Sasaki, K.; Vukmirovic, M. B.; Adzic, R. R. Palladium Monolayer and Palladium Alloy Electrocatalysts for Oxygen Reduction. *Langmuir* **2006**, *22*, 10409−10415.
(70) Blizanac, B. B.; Ross, P. N.; Marković, N. M. Oxygen Reduction on Silver Low-Index Single-Crystal Surfaces in Alkaline Solution: Rotating Ring Disk(Ag(hkl)) Studies. *J. Phys. Chem. B* **2006**, *110*, 4735−4741.
(71) Schmidt, T. J.; Stamenkovic, V.; Arenz, M.; Marković, N. M.; Ross, P. N. Oxygen Electrocatalysis in Alkaline Electrolyte: Pt(hkl), Au(hkl) and the Effect of Pd-Modification. *Electrochim. Acta* **2002**, *47*, 3765−3776.

(72) Strbac, S.; Adzic, R. The Influence of OH^- Chemisorption on the Catalytic Properties of Gold Single Crystal Surfaces for Oxygen Reduction in Alkaline Solutions. *J. Electroanal. Chem.* **1996**, *403*, 169−181.
(73) Blizanac, B. B.; Lucas, C. A.; Gallagher, M. E.; Arenz, M.; Ross, P. N.; Marković, N. M. Anion Adsorption, CO Oxidation, and Oxygen Reduction Reaction on a Au(100) Surface: The pH Effect. *J. Phys. Chem. B* **2004**, *108*, 625−634.
(74) Campbell, C. Finding the Rate-Determining Step in a Mechanism Comparing DeDonder Relations with the "Degree of Rate Control". *J. Catal.* **2001**, *204*, 520−524.
(75) Stegelmann, C.; Andreasen, A.; Campbell, C. T. Degree of Rate Control: How Much the Energies of Intermediates and Transition States Control Rates. *J. Am. Chem. Soc.* **2009**, *131*, 8077−8082.
(76) Herron, J. A.; Jiao, J.; Hahn, K.; Peng, G.; Adzic, R. R.; Mavrikakis, M. Oxygen Reduction Reaction on Platinum-Terminated "Onion-structured" Alloy Catalysts. *Electrocatalysis* **2012**, *3*, 192−202.
(77) Anderson, A. B.; Jinnouchi, R.; Uddin, J. Effective Reversible Potentials and Onset Potentials for O_2 Electroreduction on Transition Metal Electrodes: Theoretical Analysis. *J. Phys. Chem. C* **2013**, *117*, 41−48.
(78) Bligaard, T.; Nørskov, J. K.; Dahl, S.; Matthiesen, J.; Christensen, C. H.; Sehested, J. The Brønsted-Evans-Polanyi Relation and the Volcano Curve in Heterogeneous Catalysis. *J. Catal.* **2004**, *224*, 206−217.
(79) Boudart, M. Some Applications of the Generalized De Donder Equation to Industrial Reactions. *Ind. Eng. Chem. Fundam.* **1986**, *25*, 70−75.
(80) Dumesic, J. A. Analyses of Reaction Schemes Using De Donder Relations. *J. Catal.* **1999**, *185*, 496−505.
(81) Jinnouchi, R.; Kodama, K.; Morimoto, Y. DFT Calculations on H, OH and O Adsorbate Formations on Pt(111) and Pt(332) Electrodes. *J. Electroanal. Chem.* **2013**, DOI: 10.1016/j.jelechem.2013.09.031.